Soft Matter

Cite this: *Soft Matter*, 2011, **7**, 10429

www.rsc.org/softmatter

PAPER

Self-assembly and phase transformations of π-conjugated block copolymers that bend and twist: from rigid-rod nanowires to highly curvaceous gyroids†

Yi-Huan Lee,[a] Wei-Che Yen,[a] Wei-Fang Su[ab] and Chi-An Dai*[ac]

Received 21st April 2011, Accepted 19th July 2011
DOI: 10.1039/c1sm05724c

In this study, a series of π-conjugated block copolymers of regioregular poly(3-hexyl thiophene)-*b*-poly (2-vinyl pyridine) (P3HT–P2VP) was synthesized and their self-assembly behavior and the detailed thermodynamic phase diagram were explored. By a combination of TEM, SAXS, WAXS, and UV-VIS measurements, it was found that the π-conjugated P3HT in their various self-assembled nanodomains could be a rigid rod, or a semi-rigid chain, or even a fully flexible chain. With the P2VP volume fraction, ϕ, = 0.20, the P3HT–P2VP displays a nanowire structure with a fully extended all-*trans* P3HT rod structure across the width of the nanowires, indicating a prevailing rod–rod interaction between P3HT blocks over the microphase separation interaction between the constituent blocks. With ϕ = ~0.30 to 0.6, the P3HT–P2VPs show a highly ordered lamellar structure with the P3HT block exhibiting as a semirod-like chain composed of shorter rods connected by twisted 3HT units. With ϕ > 0.68, the π-conjugated block copolymers display self-assembling nanostructures of hexagonal close packed cylinders and spheres, indicating that P3HT adopts a fully coil-like structure that favors interfacial curvatures. In particular, for the P3HT–P2VP with ϕ = 0.68, a gyroid phase, the first of its kind for π-conjugated block copolymers, was observed upon heating. For the nanowire structured P3HT–P2VP, a liquid crystalline phase transition from the smectic-like crystalline state to a nematic structure was observed at ~200 °C. The observed microstructures and transformations reveal the importance of the semirigid nature of π-conjugated P3HT chains and provide new guidelines for the organization of π-conjugated block copolymers for future optoelectronic applications.

Introduction

Conducting polymers with π-conjugated backbones have gained great attention in the frontier of polymer science and technology because they possess unique optoelectronic properties for use as an active material in low-cost, large-area, and flexible optoelectronic devices. In recent years, various π-conjugated polymers including poly(*p*-phenylene) (PPP), poly(*p*-phenylene vinylene) (PPV), polyfluorene (PF) and polythiophene (PT) have been synthesized and extensively investigated.[1–3] Among them, regioregular poly(3-hexylthiophene) (P3HT) has received the most attention due to its superior charge carrier mobility, stability and processability.[4–6] Meanwhile, there has been a growing interest in the synthesis of block copolymers containing conjugated polymers since it may offer a new strategy for the organization of the π-conjugated polymers and synergistic improvements in their mechanical, optoelectronic and other properties.[7–13] For example, in photovoltaic cells, their efficiency depends critically on the charge separation and transport in the nanostructures of the devices. Thus, self-assembling conjugated block copolymers with highly ordered heterogeneous nanostructure may provide an enhanced interfacial area for charge separation and also function as an efficient pathway for charge transport.[14,15] Therefore, understanding the self-assembly behavior of these conjugated block copolymers and controlling the molecular and structural parameters that dictate the formation of their ordered microstructures are important for further improvements of new optoelectronic devices.

The thermodynamic characteristics of these novel materials are now beginning to be understood. A number of theoretical studies on the phase behavior of the so-called rod–coil block copolymers have been developed using methods including the Landau expansion theory[16–18] and the self-consistent-field theory.[19–21] These theories demonstrate that the rod–coil systems exhibit a complex self-assembly behavior which is distinctly different from that of conventional coil–coil block copolymer systems. Rod–coil systems have additional molecular parameters

[a]*Institute of Polymer Science and Engineering, National Taiwan University, Taipei, 10617, Taiwan*
[b]*Department of Materials Science and Engineering, National Taiwan University, Taipei, 10617, Taiwan*
[c]*Department of Chemical Engineering, National Taiwan University, No. 1, Roosevelt Rd. Sec. 4, Taipei, 10617, Taiwan. E-mail: polymer@ntu.edu.tw; Fax: +886-2-2362-3040; Tel: +886-2-3366-3051*

† Electronic supplementary information (ESI) available: Detailed synthesis procedures and characterizations (NMR, GPC, SAXS, WAXS and TEM) of P3HT–P2VPs. See DOI: 10.1039/c1sm05724c

which include a conformational asymmetry between the two constituent rod and coil blocks and the anisotropic interactions between the rod blocks. New experimental efforts have also shed light on the unique self-assembly behavior of conjugated block copolymers. Poly(phenylene vinylene) (PPV) based rod–coil block copolymers have been synthesized and their self-assembly behavior has also been investigated in different segregation strength regimes.[22–25] The resulting phase diagrams derived from the experimental observations are in qualitative agreement with the theoretical predictions for the rod–coil block copolymers since the conjugated block was assumed to have an effectively infinite persistence length and a single orientational director for their anisotropic interactions. However, in contrast to the assumed rigid-rod polymers such as PPV, poly(thiophene) (PT) derivatives have sufficiently high degrees of freedom that allow for a twist motion of the carbon–carbon single bond between the adjacent thiophene rings, therefore affording PT chains a semi-rigid property both in the solid state and in solutions.[26] It has been found previously that at low temperature pristine P3HT homopolymer in the solid state with adjacent thienyl units adopts a *trans*-planar conformation and exhibits a rigid-rod structure with a long persistence length. However, upon increasing the temperature, poly(3-alkyl thiophene) chains undergo a *trans* to *gauche* conversion due to the twisting motion between the adjacent thienyl units. The formation of the twisted thienyl defects (twiston) results in the conformation transformation of poly(thiophene)s from a rigid rod to a coil-like structure, which is evident from blue-shifting of their UV-VIS absorption at elevated temperatures.[27,28] Therefore, block copolymer systems containing the semi-rigid P3HT chains may exhibit different self-assembly behavior in contrast to those of the conventional rod–coil block copolymers with a fully extended rigid-rod chain conformation at low or even high temperatures. However, so far a systematic study on the equilibrium bulk structure and the phase transformations of the semirod-like P3HT based block copolymer systems have yet to be found since most studies were focused on the thin film morphology of their P3HT based block copolymers prepared *via* spin coating or drop coating with processing parameters (solvents, film thickness, drying conditions, *etc.*) that can greatly affect their thin film morphology.[12,15,29–38] Therefore, in order to fully exploit these systems for future applications, a model system of regioregular P3HT block copolymers must be synthesized and carefully characterized. In a previous study, a new anionic macroinitiation method has been developed for the synthesis of a well-defined regioregular poly(3-hexyl thiophene)-*b*-poly(2-vinyl pyridine) block copolymer system.[39] However, its detailed phase transformation has yet to be shown.

In this study, we investigated the self-assembly behavior and the detailed thermodynamic structures of the π-conjugated semi-rigid block copolymers of regioregular poly(3-hexyl thiophene)-*b*-poly(2-vinyl pyridine) (P3HT–P2VP) with different P2VP volume fractions. By a combination of transmission electron microscopy (TEM), small-angle and wide-angle X-ray scattering (SAXS and WAXS), and the solid-state UV-VIS absorption measurements on thermally annealed P3HT–P2VP samples, the detailed thermodynamic phase diagram including the order–disorder, order–order transitions of the semirod–coil P3HT–P2VP block copolymers and the liquid crystalline phase transformation of P3HT segments were revealed. Its phase diagram was found to be both significantly different from that of conventional fully rigid rod–coil block copolymers as well as that of coil–coil block copolymers. This difference has been attributed mainly to the change in the chain rigidity of P3HT due to the interplay between the π-conjugation interaction of P3HT, chain stretching and twisting of the semi-rigid P3HT and coil-like P2VP, and interfacial energy of their self-assembled nanostructure.

Experimental section

Synthesis of P3HT–P2VP block copolymers

The detailed synthesis procedures for the anionic macroinitiation method developed earlier and the characterization of the synthesized P3HT–P2VP block copolymers are described in the ESI† section. All molecular parameters of the P3HT–P2VP block copolymers used for the current study are tabulated in Table 1.

Small-angle and wide-angle X-ray scattering (SAXS and WAXS)

Samples for X-ray scattering measurements were prepared by first solvent casting a 10 wt% polymer solution onto a 1 mm thick washer, followed by a slow evaporation of the solvent for several days. The washer samples were then placed between two Kapton® sheets to prevent sample leakage at higher temperature. The sealed samples were annealed at 220 °C for 5 minutes to remove any thermal history as verified by SAXS and WAXS

Table 1 Summary of the molecular characteristics of P3HT–P2VP samples

Sample[a]	M_n/g mol^{-1}, P3HT	M_n/g mol, P2VP	PDI	f^b	SI transition (WAXS)	T_{ODT} (SAXS)
P3HT	6800	—	1.17	0		
HTVP20	6800	1600	1.27	0.20	—	220 ± 5[c]
HTVP29	6800	2600	1.25	0.29	190 ± 5	210 ± 5
HTVP46	6800	5600	1.22	0.46	160 ± 5	200 ± 5
HTVP57	6800	8600	1.19	0.57	140 ± 5	180 ± 5
HTVP68	6800	13 800	1.16	0.68	—	160 ± 5
HTVP76	6800	20 400	1.19	0.76	—	180 ± 5
HTVP87	6800	41 800	1.18	0.87	—	—

[a] HTVP: designation of P3HT–P2VP block copolymers. Based on the ^{1}H-NMR spectrum shown in Fig. S3 of the ESI†, the regioregularity of a P3HT block is estimated to be ~0.93. [b] The volume fraction of P2VP in P3HT–P2VP calculated based on the density values of 1.10 g cm^{-3} for P3HT and of 1.14 g cm^{-3} for P2VP. [c] T_{ODT} of HTVP20 was estimated from the TEM measurement.

measurements that show the disordered melt state for P3HT–P2VP samples (see Fig. S7 in the ESI†). The melted samples were subsequently cooled slowly to 130 °C at a rate of 1 °C min^{-1} and annealed at that temperature for 3 days under a high vacuum environment (10^{-6} torr) in order to obtain the thermodynamic equilibrium. During the slow cooling process, P3HTs in the copolymers were allowed to crystallize in the nanostructure that the P3HT–P2VP adopts. The final annealing temperature of 130 °C was chosen because it is above the glass transition temperature of P2VP such that the equilibrium can be reached. SAXS and WAXS experiments were performed separately at the 23A1 and 13A1 endstations of the National Synchrotron Radiation Research Center (NSRRC) of Taiwan. The wavelength of the incident beam was 1.18095 Å for the SAXS and 1.03051 Å for the WAXS measurements. For the temperature scan of the X-ray spectra, the annealed samples were heated in-line with a PID controlled heating unit to a specified temperature under a dried nitrogen environment for 10 min before the X-ray spectra are collected.

Transmission electron microscopy (TEM)

Samples for the bulk equilibrium morphology measurements using TEM were annealed by following the same sample preparation procedure as that for SAXS and WAXS measurements. The thermally equilibrated sample block was cut into thin films of <100 nm thickness using a Reichert Ultracut microtome with a diamond knife. The cut samples were stained by exposing them to the vapor of iodine for 12 hours. Bright field TEM measurement was performed using a JEOL 1230EX transmission electron microscope operating at 120 kV with a Gaten Dual Vision CCD Camera on samples for the bulk morphology.

Differential scanning calorimetry (DSC)

All DSC measurements were carried out using a Perkin-Elmer Diamond® differential scanning calorimeter equipped with an intracooler. All samples, typically ~5 mg, were sealed in aluminium pans for the analysis. The measurements were carried out by first heating the samples to 220 °C at a heating rate of 10 °C min^{-1}, then keeping the samples at that temperature for 5 minutes to erase any thermal history of the samples. The annealed samples were then cooled to 0 °C slowly at a rate of 2.5 °C min^{-1} for the self-organization of the polymer samples. Finally, a reheating of the sample at a rate of 10 °C min^{-1} was performed and the thermogram was recorded.

Optical property analysis

The UV-VIS absorption and photoluminescence (PL) measurements of P3HT–P2VP block copolymers in the solid state were conducted using a JSACO V-570 UV/VIS/NIR spectrophotometer and a JSACO FP-6300 spectrophotometer at room temperature. The excitation wavelength for the PL measurements was chosen to be 380 nm aimed for P3HT absorption in this study. The samples for the UV-VIS absorption and photoluminescence studies were prepared by using the same sample preparation and annealing procedures as those for the TEM measurements.

Results and discussion

Morphology and self-assembly behaviors

The morphology of P3HT homopolymer has been known to be affected by their strong π–π interaction between the conjugated backbones, leading to the formation of highly ordered molecular organizations. Therefore, in addition to the enthalpic interaction characterized by the Flory–Huggins interaction parameter, χ, between different constituent blocks, the phase diagram and the molecular arrangement of P3HT-based block copolymers in the condensed phase are therefore also affected by the Maier–Saupe parameter (μ) which characterizes the rod–rod interactions. Since, for the current P3HT–P2VP system, the molecular weight of the P3HT block was kept constant while the molecular weight of P2VP block was varied, the relative strength of microphase separation (χN_{total}) to the orientational ordering between P3HT blocks (μN_{P3HT}) will be accessed by changing the P2VP molecular weight, where N_{total} is the total degree of polymerization for the block copolymers. Here, we report the details on the morphological investigations and structural identifications of the thermally annealed P3HT–P2VP block copolymers with different volume fractions by employing the combination of TEM, SAXS, WAXS and solid state UV measurements. Shown in Fig. 1(a), (c), (e) and (g) are the representative TEM micrographs of the solvent cast HTVP20 (with 20% of P2VP), HTVP29, HTVP68, and HTVP87 samples, respectively, before the thermal annealing for equilibrium. The dark region in the TEM micrograph corresponds to a P2VP domain stained with iodine while the white region corresponds to a P3HT domain without any iodine staining. From all of the above TEM micrographs, a fibril structure or nanowire morphology was observed with a decreasing number density of fibrils present in the micrographs with an increasing P2VP fraction from HTVP20 to HTVP87. The fibril structure shows a great resemblance to those observed in solvent-cast thin films of other P3HT based block copolymer systems with a wide range of P3HT compositions from several previous studies.[12,15,29–38] The morphology and phase transition of the thermally annealed P3HT–P2VPs are the current focus of this study and are presented as follows.

A. Fibril structure for $\phi \leq 0.2$. The TEM image of the thermally annealed HTVP20 block copolymer sample is shown in Fig. 1(b). From the TEM micrograph, the fibril structure or the nanowire morphology was also observed after the thermal annealing. The nanowires appear to be orienting randomly yet extending along its fibril long-axis for several hundred nanometres. The average diameter of the nanowires was estimated from the TEM micrograph and was found to be around 16–18 nm. The corresponding SAXS spectrum for HTVP20 shows that there is only a very shallow and barely visible scattering peak shown in the top curve of Fig. 2(a). A calculation for the diameter of the nanowires based on this scattering peak position (q^*) also gives a characteristic structural spacing of around 20 nm, close to the TEM measurement shown in Fig. 1(b). The observation of a nanowire structure for block copolymers containing P3HT is not surprising since P3HT homopolymer has been known to exhibit a fibril structure.[40] As stated earlier, a similar fibril structure has also been reported in other block copolymer

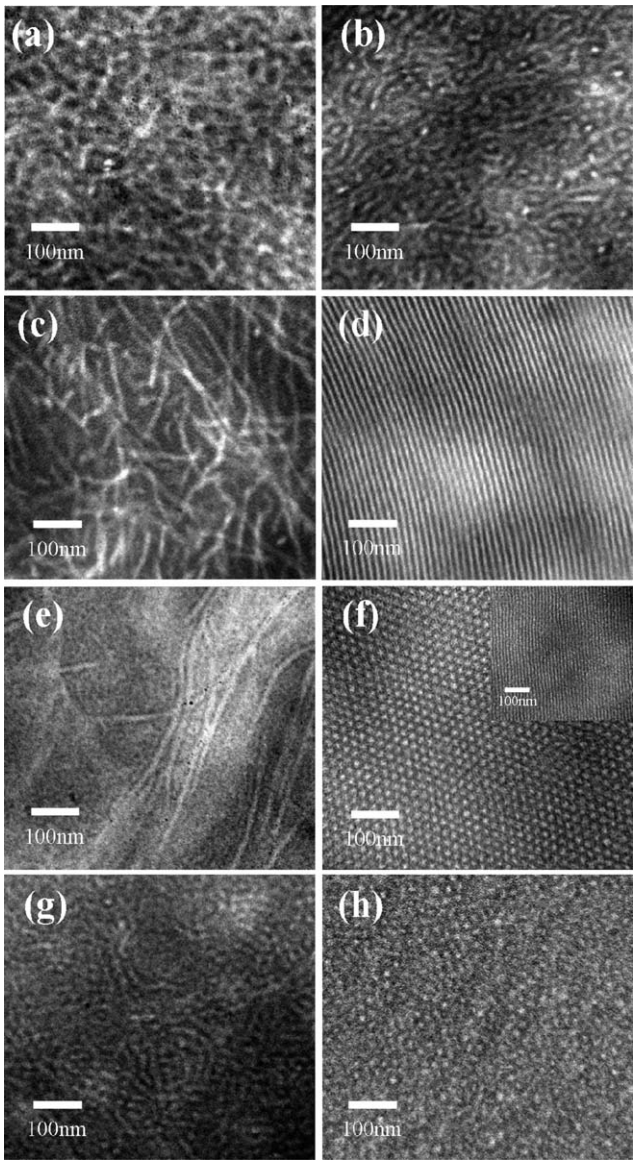

Fig. 1 TEM micrographs of solvent-cast samples of (a) HTVP20, (c) HTVP29, (e) HTVP68, and (g) HTVP87. Nanofibrils are clearly visible in the above samples prepared by using just the solvent casting process. After thermal annealing at 130 °C the above nanofibril structured samples transform into (b) the nanofibril structure of HTVP20, (d) the lamella structure of HTVP29, (f) the cylinder structure of HTVP68, and (h) the sphere structure of HTVP87. The inset in (f) shows the side view of the thermally annealed HTVP68 cylinders.

systems containing P3HT. McCullough *et al.* and others have reported the presence of the fibril morphology for a solvent-cast thin film of a rod–coil block copolymer containing P3HT.[29,30] They have been attributing the presence of this self-assembling nanostructure to a kinetic trapping effect that is inherent to the solvent-casting procedure. However, the fibril morphology we observed for HTVP20 in the current study was from bulk samples that have been thermally treated. As described in the Experimental section, all TEM/SAXS/WAXS/UV samples were first solvent cast, dried in high vacuum, and heated to 220 °C to remove any thermal history followed by annealing the samples at 130 °C for equilibrium. Therefore, both thermally annealed and solvent cast HTVP20 samples exhibit a rather similar fibril structure. Furthermore, the fibrillar structure of HTVP20 is indeed thermally reversible. The copolymer self-assembles into a fibril structure after annealing at 130 °C for 24 hours as shown in Fig. 3(a). A decrease in the fibril length is seen as the copolymer is annealed at 180 °C for 24 h (Fig. 3(b)). Fig. 3(c) shows that the 220 °C sample exhibits a disordered structure that is free of fibrils but a disordered region with contrast between P3HT and P2VP in the range of ~20 to 30 nm is still visible. However, upon cooling the sample from 220 °C, the reappearance of the fibril structure is seen for HTVP20, shown in Fig. 3(d). Therefore, it shows that the nanowire phase is indeed a thermodynamically stable structure with a thermally reversible "order–disorder" phase transition. The formation of the fibril structure may be resulted from a unique property of P3HT that strong π–π interactions between P3HT chains favor the formation of its crystal structure (XRD results shown later) consisting of P3HT all-*trans* stiff main chains. This crystal structure then dominates over the microphase separation interaction between the P3HT rod and the short P2VP coil ($\mu N_{P3HT} > \chi N_{total}$). Although further investigation is still needed to understand the intrinsic property of the nanofibrillar structure, the observed morphology supports the conclusion of the importance of the rod–rod interaction that favors a thermally stable nanofibrillar structure in the current conjugated block copolymer system at low coil fraction.

B. Lamellar structure for $0.29 \leq \phi \leq 0.57$. With a wide range of the P2VP coil fraction from $\phi = 0.29$ to 0.57, the thermally annealed P3HT–P2VP block copolymers organize into a uniform lamellar phase. Fig. 1(d) shows the TEM image of HTVP29. Note that HTVP29 displays a lamellar nanostructure, which is in contrast to many coil–coil block copolymers that often exhibit a cylindrical structure at the same volume fraction. This difference in the self-assembled nanostructure may be due to the differences in the chain conformation of P3HT chains compared with other random coiled polymers. The bottom three curves in Fig. 2(a) show the SAXS patterns for HTVP29, HTVP46, and HTVP57 with peaks located at integer multiples of its first scattering peak position, q^*. The presence of higher order peaks in those curves demonstrates the existence of a macroscopically highly ordered lamellar structure for all three block copolymers. In particular, HTVP46 shows the first scattering peak signal at $q^* = 0.04$ (1/Å) and another relatively weak but clearly visible peak signal at $3q^*$. The disappearance of the $2q^*$ reflection for HTVP46 indicates that the lamellar structure exhibited by HTVP46 is nearly symmetrical. With increasing P2VP fraction from HTVP29 to HTVP46 and to HTVP57, their first scattering peak position q^* moves to a smaller angle which corresponds to a larger lamellar long-spacing. Based on the Bragg's law, their measured long spacings are 13.3 nm, 14.9 nm, and 15.7 nm for HTVP29, HTVP46, and HTVP57, respectively.

C. Hexagonal cylinders, and disorder micelles for $0.68 \leq \phi$. With the P2VP coil fraction = 0.68 to 0.76, the P3HT–P2VP block copolymers self-assemble into a highly ordered hexagonal packed phase. Fig. 1(f) shows the TEM image of HTVP68 where the unstained white region corresponds to the P3HT domain that forms the inner cylinder while the dark region corresponds to the

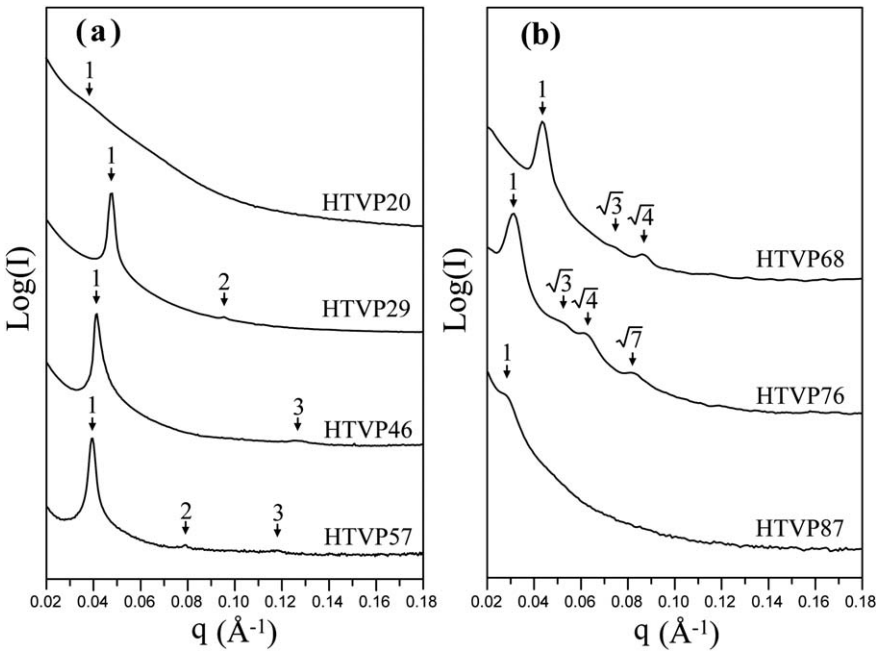

Fig. 2 (a) SAXS spectra for HTVP20, HTVP29, HTVP46, and HTVP57 that show the microstructure of nanofibril for HTVP20 and the lamellar structure for HTVP29, HTVP46, and HTVP57. (b) The SAXS spectra for HTVP68 and HTVP76 of the hexagonal cylinder structure and for HTVP87 of the spherical structure.

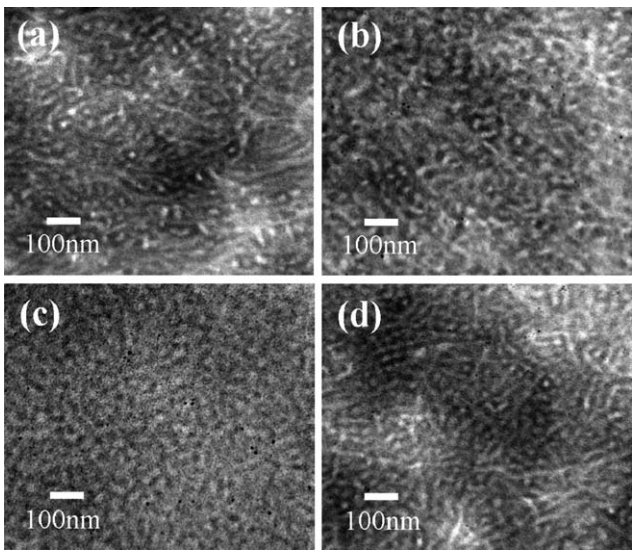

Fig. 3 TEM micrographs of HTVP20 annealed at different temperatures. (a) The copolymer self-assembles into a fibril structure after annealing at 130 °C for 24 hours followed by rapid quenching in liquid nitrogen; (b) a view of the HTVP20 sample quenched from 180 °C annealing for 24 h to liquid nitrogen; (c) a view of the disordered structure of a HTVP20 sample quenched from 220 °C annealing for 24 h to liquid nitrogen and (d) the reappearance of the fiber-like structure of a HTVP20 sample quenched from the melt to liquid nitrogen and annealed at 130 °C for 24 h in a high vacuum oven.

P2VP domain that forms the outer continuous phase. The side view of the hexagonal cylinder phase showing the column-like structure could be found for HTVP68. As shown in the inset of Fig. 1(f), strips with alternating light and dark contrast of a column-like structure of the hexagonal phase are observed for HTVP68. Note that the microstructure of the P3HT–P2VP block copolymers containing high P2VP coil fractions resembles that of conventional coil–coil block copolymers despite the fact that P3HT–P2VP with low P2VP fractions are considered as more of a rigid rod–coil block copolymer system (*e.g.* HTVP20 and HTVP29). The SAXS pattern of HTVP68 shown as the top curve in Fig. 2(b) reveals the peak position of the diffraction reflections at ratios corresponding to ordered cylinders in a hexagonal lattice: $q/q^* = 1$, $\sqrt{3}$ and $\sqrt{4}$, consistent with the corresponding TEM measurements. Similar to HTVP68, HTVP76 also self-assembles into a hexagonal packed phase and its structure can be identified by SAXS, as shown in Fig. 2(b). The *d*-spacings as determined from the first peak of their scattering patterns of HTVP68 and HTVP76 are measured and found to be 14.6 nm and 20.2 nm, respectively. The *d*-spacing of the hexagonal cylinder phase increases monotonically with the P2VP fraction as expected.

With a highest P2VP coil fraction of 0.87, we observed that the thermally annealed HTVP87 sample exhibits a disordered micelle or spherical phase, as shown in Fig. 1(h). The microstructure of the HTVP87 bulk sample was also identified by using SAXS measurements and the spectrum is shown as the bottom curve in Fig. 2(b). In the scattering pattern, only a weak peak centered at a value in the scattering wave vector q corresponding to ~22.8 nm of the interparticle spacing of the micelles is observed. No other higher order reflections are visible for HTVP87.

Gyroid phase and order–order/order–disorder transitions

Besides HTVP20 exhibiting a fibrillar order–disorder transition, P3HT–P2VPs with different P2VP volume fractions also show diverse self-assembling structures that undergo a thermally

reversible order–disorder or even order–order transition. The order–disorder and order–order phase transitions of the P3HT–P2VP block copolymers were characterized by using in-line step-wise heating and cooling of the samples during SAXS measurements. Fig. 4(a) and (c) show the effect of annealing temperature on the scattering patterns of the lamellar structured HTVP29 and the HCP structured HTVP68, respectively. As the temperature is increased to ~210 °C, the intensity of the primary peak of HTVP29 suddenly decays while the higher order peak ($2q^*$) disappears completely. Therefore, at ~210 °C there is an ordered lamellae-to-disordered phase transformation for HTVP29. Above 210 °C, the residual primary peak is still visible due to the local density fluctuation of the two components of the block copolymer in the disordered phase.[41] Notably, for HTVP68 upon heating to temperatures of about 140–150 °C we observe that the diffraction peaks characteristic of a hexagonal cylinder structure

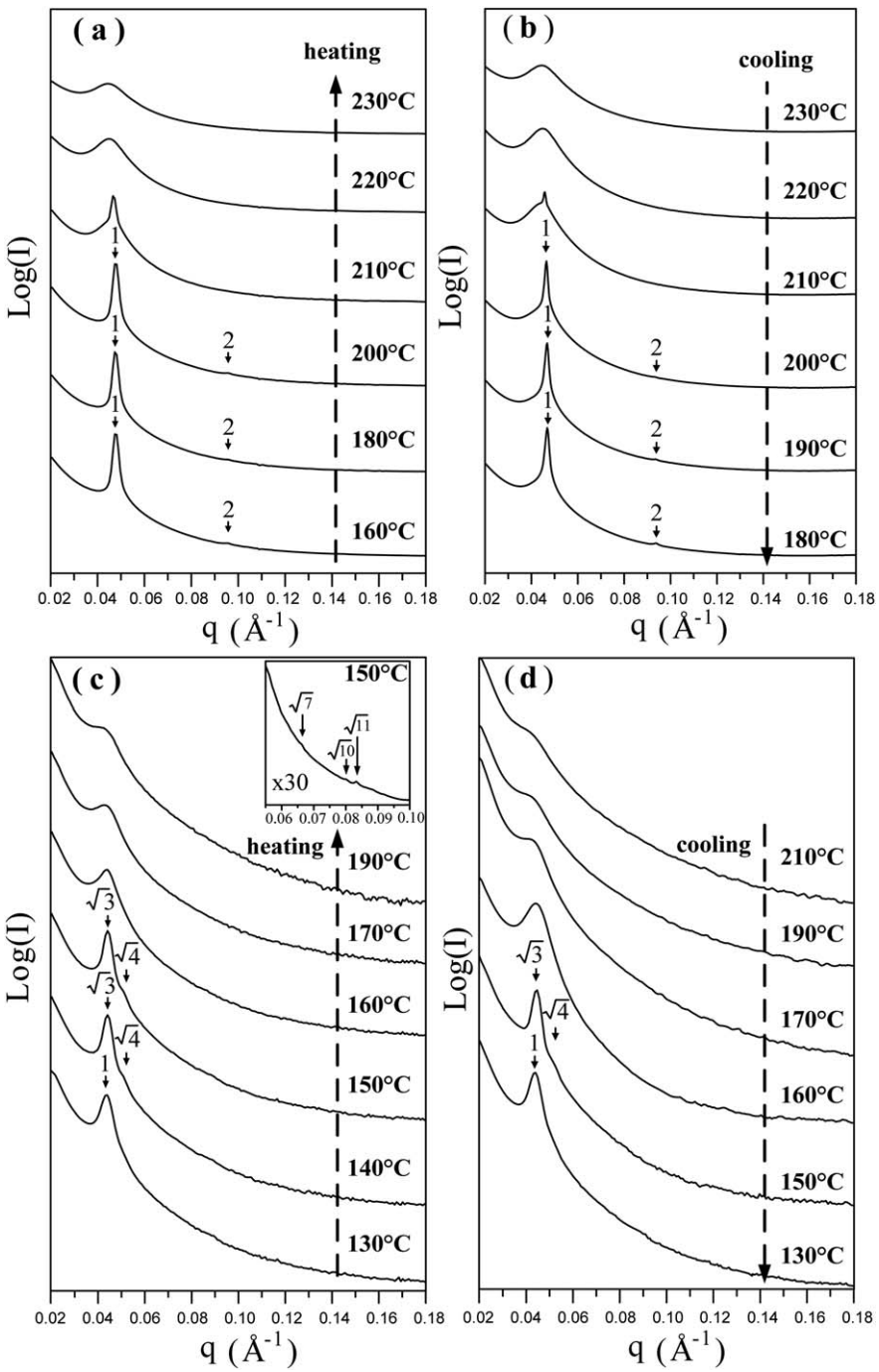

Fig. 4 The step-wise heating SAXS spectra for (a) HTVP29 and (c) HTVP68 samples. After the samples were melted, step-wise cooling SAXS spectra were collected for (b) HTVP29 and (d) HTVP68. The SAXS profiles observed during the heating and cooling processes demonstrate a thermally reversible order–disorder transition. The inset shown in (c) exhibits higher order scattering peaks associated with a gyroid structure for HTVP68 annealed at 150 °C.

vanish and a new set of peaks appear at peak ratios of $\sqrt{3}q^*$ and $\sqrt{4}q^*$. High order scattering peaks for HTVP68 annealed at 150 °C are also seen as shown in the inset of Fig. 4(c). The dramatic change in the scattering pattern signifies an order–order transition (OOT) at which the block copolymers phase transform from an ordered cylinder phase to another ordered phase with the exact structure to be determined later. Upon further heating above 160 °C, an order–disorder transition (ODT) was found which is characterized by a drop in the intensity of the primary scattering peak ($\sqrt{3}q^*$) and the disappearance of the higher order peak ($\sqrt{4}q^*$). If the observed nanostructures are at the thermodynamic equilibrium, they should be reversible upon cooling from the disordered melt. Therefore, in addition to the step-wise heating experiment, in-line step-wise cooling experiments on SAXS line for HTVP29 and HTVP68 samples from the disordered melt were also performed. Fig. 4(b) and (d) show the variation of SAXS spectra as a function of temperature during the cooling process for the lamellar structured HTVP29 and the HCP structured HTVP68, respectively. As the sample is initially heated to 230 °C, the SAXS spectrum of HTVP29 shows only a broad but weak primary peak, indicating a disordered phase at this temperature. As the temperature is decreased to ~210 °C, the intensity of the primary peak of HTVP29 suddenly increases while the higher order peak ($2q^*$) begins to appear. Therefore, at ~210 °C there is a disordered to ordered lamellae transformation for HTVP29. Additionally, for HTVP68 upon heating to temperatures of about 190–210 °C, we observe the diffraction peaks characteristic of a disordered state. As the temperature is decreased to ~160 °C, a disorder to order transition (ODT) was found due to a new set of peaks appeared at peak ratios of $\sqrt{3}q^*$ and $\sqrt{4}q^*$ in the SAXS spectrum. Therefore, below 160 °C there is a disordered phase to ordered gyroid phase transformation for HTVP68. As the temperature is further decreased to ~130 °C, there is an ordered gyroid structure to ordered hexagonal cylinder phase transformation for HTVP68. On the basis of the temperature-dependent SAXS data, we observe that the SAXS results on the cooling process are qualitatively consistent with those on the heating process. Remarkably, the observed microstructures in our study are at thermodynamic equilibrium states, therefore, the temperature-dependent SAXS spectra are reversible upon cooling from the disordered melt.

In order to fully determine the equilibrium microstructure of this copolymer as a function of temperature, the ordered microstructures of HTVP68 were investigated by using TEM. The HTVP68 bulk sample was prepared by annealing it at different temperatures followed by quenching the samples into a liquid nitrogen bath in order to preserve the morphology obtained at the annealing temperature. Fig. 5(b) and (c) show that HTVP68 self-assembles into an interpenetrating phase at 150 °C and a disordered phase at 220 °C, respectively. In particular, the new structure shown in Fig. 5(b) exhibits a four-fold projection of a bicontinuous structure which is consistent with a gyroid ($Ia\bar{3}d$) structure typically occurring only in a narrow range of volume fraction between a hexagonal cylinder phase and a lamellar phase of coil–coil block copolymer systems.[42,43] Additionally, the inset in Fig. 5(b) shows an image of the three-fold projections of the gyroid ($Ia\bar{3}d$) structure of HTVP68 equilibrated at 150 °C. Therefore, the characteristic SAXS patterns and the corresponding TEM images demonstrate

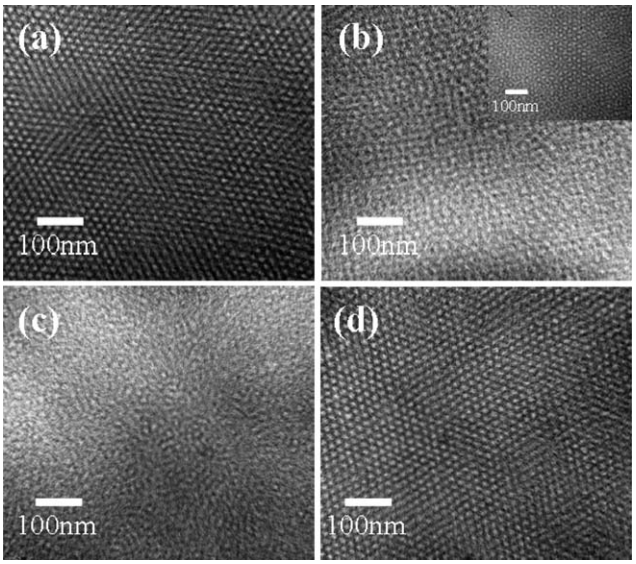

Fig. 5 TEM micrographs of HTVP68 annealed at different temperatures. The copolymer self-assembles into (a) hexagonal close-packed cylinders after annealing at 130 °C for 24 hours followed by rapid quenching in liquid nitrogen, (b) a gyroid phase (4-fold projections) after annealing at 150 °C for 24 hours followed by rapid quenching in liquid nitrogen, (c) a disordered phase after annealing the sample at 220 °C for 24 hours followed by rapid quenching in liquid nitrogen, and (d) hexagonal close-packed cylinders after cooling from 220 °C and annealing at 130 °C for 24 hours followed by rapid quenching in liquid nitrogen. The inset in (b) shows the 3-fold symmetry pattern of the gyroid ($Ia\bar{3}d$) phase.

the presence of a gyroid ($Ia\bar{3}d$) structure for our current π-conjugated P3HT–P2VP block copolymer system. According to our knowledge, this is the first example of a π-conjugated diblock copolymer which exhibits hexagonal cylinders and a gyroid phase through an order–order transition. The discovery of a gyroid phase in a conjugated block copolymer system is surprising since a gyroid phase may require domain interfaces with high degrees of curvature. Furthermore, the existence of a bicontinuous phase for rod–coil diblock copolymers has neither been predicted by theories nor been observed by experiments since a fully rigid-rod nature of the conjugated block was often assumed. Remarkably, the semi-rigid nature of regioregular P3HT results in the change in the chain conformation with the P2VP molecular weight, therefore, affecting the degree of freedom of the rotation about the interannular bond of the P3HT block and imparting a profound effect on the self-assembling behavior and shows a wealth of different phases.

To summarize the above result, the transition temperatures of all the block copolymers are listed in Table 1. Note that the HTVP68 sample has the lowest T_{ODT}, which may be resulted from the induced instability at high temperatures for the gyroid structure with large curvatures.[44]

Optical properties

The photophysical property of the P3HT homopolymer and P3HT–P2VP block copolymers in the solid state was also measured. Fig. 6(a) shows the UV-VIS absorption spectra of the

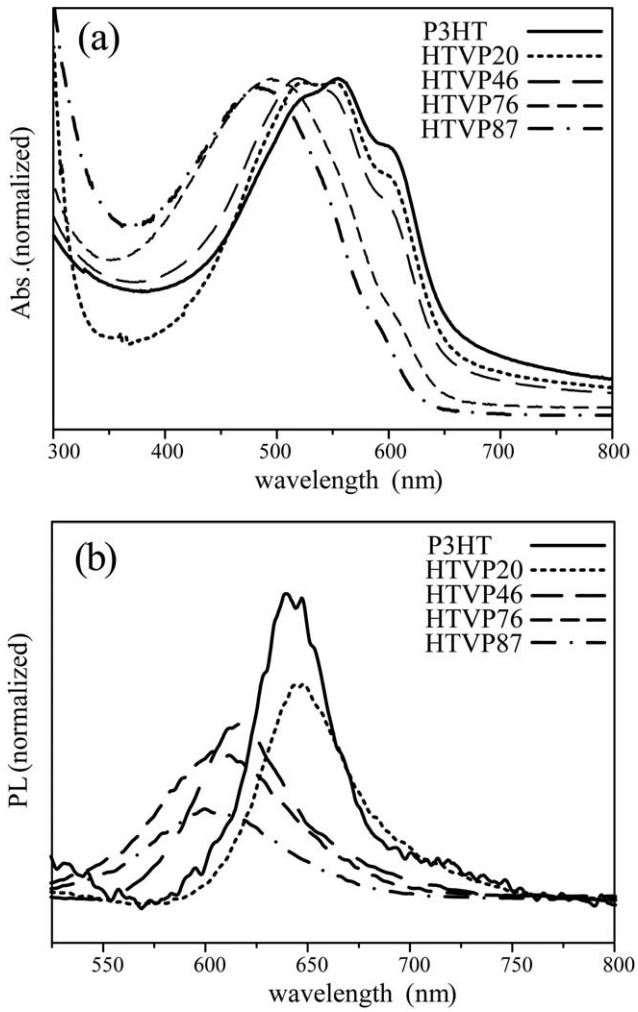

Fig. 6 (a) UV-VIS absorption spectra and (b) PL spectra of P3HT and P3HT–P2VP thin films. P3HT homopolymer (—), HTVP20 (···), HTVP46 (— —), HTVP76 (**---**), and HTVP87 (**-·-**).

film samples. The UV-VIS spectra show that HTVP20 and P3HT homopolymer have almost the same $\lambda_{max,UV}$ value of around 557 nm. The effect of more P3HT chain aggregation is also evident from the presence of an additional absorption shoulder appearing at longer wavelengths around 605 nm than its $\lambda_{max,UV}$ in the film samples.[45] The result clearly indicates that the chain conformation of the P3HT block of HTVP20 in the solid state exhibits a similar *trans*-planar conformation which favors long conjugation lengths to that of the P3HT homopolymer. However, the UV-VIS spectrum of the HTVP46 film shows that its $\lambda_{max,UV}$ is largely blue-shifted to 520 nm compared to that of the HTVP20 film. The shifts in the absorption maximum are likely due to a change in the conjugation length of the P3HT chains in the HTVP46 block copolymer film. Even though HTVP20 and HTVP46 have the same molecular weight (M_n = 6800) in their P3HT block, the larger molecular weight of P2VP chains in HTVP46 can presumably affect in greater extent the chain conformation of the P3HT block since the P2VP block is in close proximity to the P3HT chromophore that affects how P3HT is packed in the solid state. As shown previously from TEM and SAXS measurements, the synthesized P3HT–P2VP block copolymer with different P2VP fractions formed different microstructures that could lead to a different packing state of the P3HT block, resulting in the change of the absorption characteristics. Since HTVP46 shows a blue-shifted $\lambda_{max,UV}$, its P3HT block adopts a less planar main-chain conformation in lamellae than that of P3HT in fibrillar HTVP20. As the P2VP coil fraction increases further from 0.46 to 0.76, we observe more blue-shifting of the absorption maximum from 525 nm to 498 nm, indicating that the P3HT in HTVP68 exhibits an even shorter conjugation length than that of the lowered P2VP fraction samples. As the P2VP fraction further increases to a value of 0.87, the absorption peak of the P3HT–P2VP is blue-shifted to 487 nm. Therefore, with the increasing P2VP coil fraction, there is a progressing decrease in the absorption maximum for the block copolymer film samples with $\phi \geq 0.46$. In addition, photoluminescence measurements in the solid state also show a similar trend in $\lambda_{max,PL}$. As shown in Fig. 6(b), there is a hypsochromic shift in $\lambda_{max,PL}$ for all block copolymers with increasing P2VP fractions except for HTVP20. The PL result is consistent with the UV-VIS absorption result. In summary, from the above measurements we can conclude that with the small P2VP coil fraction ($\leq\sim$0.2) the P3HT chains adopt a *trans*-planar main-chain conformation that favors a strong π–π interchain interaction, therefore, without any blue-shifting of their absorptions. With increasing P2VP coil fractions above 0.2, however, there seems to be a conformational transformation of P3HT segments from a rod-like structure with a long conjugation length to a chain structure with a shorter conjugation length. This result suggests that the rigidity of the conjugated P3HT chains can be adjusted by changing the P2VP molecular weight of the block copolymers. Therefore, the way P3HT blocks pack within its domain may be more complicated than that of permanently rigid rod polymers due to the interplay between the π–π interaction of main chain backbone and an entropic effect associated with the flexibility of P3HT segments. In this paper, a detailed study of the self-assembly of P3HT–P2VP copolymers will be described in the following sections.

Molecular packing of P3HT in nanodomains. The ordered structure of many conjugated polymers was previously found to be closely related to the degree of dense stacking of their conjugated main-chain backbones separated by a more disordered side chain layer, resulting in the formation of solid crystal and liquid crystalline phases at high temperatures.[3] Therefore, the determination of molecular packing for conjugated chains is needed for the purpose of constructing a complete phase diagram for their corresponding block copolymers. In the present study, the molecular packing of P3HT chains within the microphase separated domains was determined by wide-angle X-ray scattering and the solid state UV-VIS absorption measurement shown in the previous section.

As shown in Fig. 7(a), we observed that the WAXS patterns of both the P3HT homopolymer and the HTVP20 exhibit similar diffraction peaks, which correspond to the reflections from the crystallographic planes of (100), (200), (300) and (020) associated with a regular form I crystal of an orthorhombic unit cell.[46,47] For the P3HT homopolymer, its corresponding *d*-spacings of (100) and (020) planes are 17.1 Å and 3.8 Å, respectively. The (100) reflection corresponds to the interlayer distance separated by the alkyl side chain of P3HT and the (020) reflection corresponds to

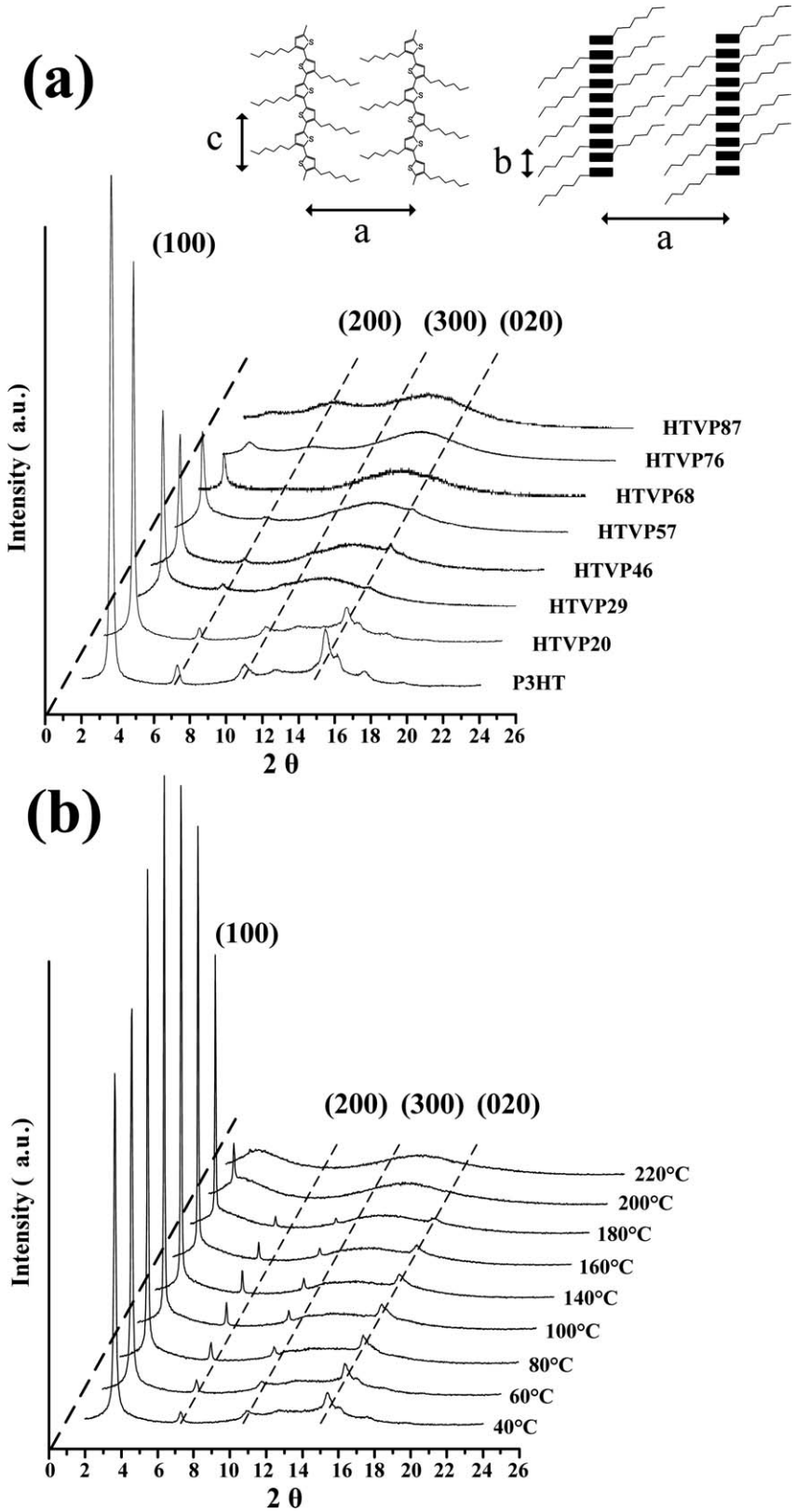

Fig. 7 (a) The room temperature WAXS spectra of thermally annealed P3HT homopolymer and P3HT–P2VP block copolymers. The inset shows the form I structure of a P3HT crystal. (b) The change in the WAXS profiles of HTVP20 is seen during a step-wise heating process.

the distance of the stacking between the main chain layers. The solid state UV-VIS spectra shown in Fig. 6(a) indicate that the P3HT block of HTVP20 adopts a *trans*-planar main-chain conformation which favors a long conjugation length and a large persistence length, similar to that of the pristine P3HT homopolymer since both the P3HT homopolymer and HTVP20 have almost the same UV absorption profile. Therefore, it can be expected that the packing of P3HT blocks in HTVP20 nanofibrils is highly ordered due to a strong attractive interaction between P3HT main-chain backbones in comparison with the segregation strength exhibited between P3HT and P2VP blocks for HTVP20 ($\mu N_{P3HT} > \chi N_{total}$). A theoretical all-*trans* chain length of the P3HT block can be obtained by multiplying the monomer unit length (0.39 nm)[48] with the degree of polymerization of P3HT ($N_{P3HT} = 41$) to give a rod length of 16 nm, which is in accordance with the TEM measurement of the width of the nanowires shown in Fig. 1(b). More importantly this result further demonstrates that the molecular organization of P3HT chains in nanofibrils consists of a monolayer of P3HT rods.

For higher P2VP fraction samples, the WAXS patterns of the lamellar structured samples of HTVP29, HTVP46 and HTVP57 also exhibit (100), (200), (300) and (020) diffraction peaks, although with reduced intensities. The solid state UV-VIS measurements show that the $\lambda_{max,UV}$ of the block copolymers was progressively blue-shifted with increasing PVP fractions relative to that of the homopolymer P3HT, indicating a decrease in the conjugation length. From the TEM measurement, we have also found that the P3HT domain size (~7 to 8 nm) of the lamellar structured samples is smaller than the all-*trans* fully extended P3HT chains of the nanofibril structure (~16 nm). These results combine to indicate that P3HT in the lamellar domain exhibits a segmented rod-like chain structure which consists of shorter rods connected by twisted thienyl units yet the neighboring P3HT shorter rods may form crystals within their nanodomain. The ordered crystal domains are separated by disordered domains which harbor structural defects like chain bends or folds.

For the cylindrical structured HTVP68 and HTVP76, only a weak and broad (100) diffraction peak is visible in the WAXS patterns, indicating a poor packing of P3HT segments in the cylinder nanostructure. This may be resulted from the combined effects of prevailing microphase separation over orientational ordering ($\chi N_{total} > \mu N_{P3HT}$) with increasing P2VP molecular weights and the two-dimensional confinement effect of the cylinder structure on the molecular packing of P3HT chains. The absorption maximum of the cylinder structured HTVP68 was also significantly blue-shifted compared with that of the P3HT homopolymer (see in Fig. 6(a)), suggesting that the P3HT blocks in the cylindrical microstructure adopt a less planar and twisted main-chain conformation. Therefore, from the above measured X-ray results, for HTVP68 and HTVP76, their P3HT blocks appear to exhibit a coil-like chain structure in the cylindrical microstructure. It should be noted that the coil-like P3HT chains in cylindrical domains are consistent with the presence of a gyroid ($Ia\bar{3}d$) phase observed at a high temperature near T_{ODT} of HTVP68. Upon heating, the P3HT chains further coil up and create more curvature at the P3HT/P2VP interface. Therefore, it is evident that at low coil fractions the P3HT in the HTVP block copolymers can be considered as a fully rigid rod to a segmented rod-like chain while at high coil fractions, P3HT acts as a fully coil-like polymer chain. For the highest P2VP coil fraction, the HTVP87 sample exhibits a fully coil-like structure with no crystalline peak in the WAXS pattern. The corresponding solid state UV-VIS spectrum of the HTVP87 sample shows that the P3HT has the smallest conjugation length, and therefore, exhibits the largest blue-shifted absorption maximum. It is difficult to obtain an even higher degree of order of the spherical structure of HTVP87 at higher segregation strength since the annealing temperature of HTVP87 is close to the T_g of the P2VP block (~100 °C).

In order to further characterize the geometric confinement effect of the nanostructure on P3HT stacking, the thermal property of the synthesized block copolymers was measured by using differential scanning calorimetry (DSC). The DSC thermograms for P3HT homopolymer and P3HT–P2VPs are shown in Fig. 8. For the pure P3HT homopolymer, there is an endothermic peak with a low temperature shoulder appearing in the temperature range between 180 °C and 215 °C in the DSC thermogram, indicating a two-stage melting of P3HT segments. The endothermic shoulder at a lower temperature of ~190 °C appears to correspond to the reported transition of P3HT ordered packing melting to a nematic phase and the main endothermic peak centered at a higher temperature of ~210 °C then corresponds to the nematic-to-isotropic phase transition.[49] For HTVP20, its DSC curve shows a similar endothermic transition as that of the pure P3HT homopolymer, indicating that the heating process also results in a series of transitions from the well-packed smectic-like crystals to nematic and to isotropic phases with increasing temperature. The DSC thermogram of

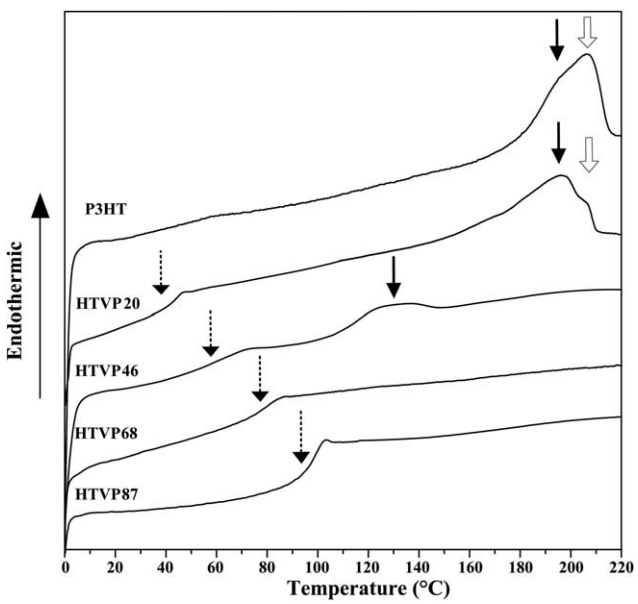

Fig. 8 DSC traces of the P3HT–P2VP block copolymers. The 2nd heating thermograms of P3HT homopolymer, HTVP20, HTVP46, HTVP68 and HTVP87 are shown. The dashed arrows indicate the glass transition temperature of the P2VP block, the solid arrows show the endothermic transition associated with the melting of the P3HT crystals, and the hollow arrows indicate the endothermic enthalpy peak associated with the nematic-to-isotropic phase transformation.

HTVP46 exhibits a melting endothermic peak at lower temperature than that of HTVP20. This decrease in the transition temperature indicates that the segmented rod-like P3HT blocks in the lamellar structured HTVP46 exhibit a less ordered packing structure than the P3HT rods in the nanofibrillar structured HTVP20. For $\phi \geq 0.68$ no endothermic peak was observed in the DSC thermogram. This may be in part due to low sensitivity of the DSC technique and in part due to a much reduced crystallinity of P3HT obtained in the cylindrical and spherical microstructures. The above result is also consistent with the conclusion from WAXS and UV-VIS measurements for high coil fraction block copolymers. As a consequence, the decrease in the melting temperature with increasing ϕ gives an indication of the relative stability of the ordered phases in different self-assembled structures.

The effects of temperature on the crystal structure and the stability of P3HT chains in their nanodomain were also investigated using in-line heating WAXS measurements. Fig. 7(b) shows a representative WAXS pattern of HTVP20 as a function of temperature and displays the diffraction peaks corresponding to the (h00) and (020) planes. As the sample is heated to 80 °C, changes in the diffraction patterns were observed; a shift in the (h00) peak position to lower angles, a shift in the (020) peak position to higher angles, an increase in the (h00) reflection intensity and the sharpening of these diffraction peaks are simultaneously observed. The above results demonstrate that upon melting of the alkyl side chain of P3HT chains at 80 °C there is a reordering of the P3HT crystals in the HTVP20 sample due to the strong π–π interaction between P3HT blocks. Upon further heating to ~160 °C, the intensity of (h00) and (020) reflections starts decreasing, indicating a decrease in the lateral ordered packing of P3HT and the loss of π–π stacking between P3HT main chains. This result suggests the formation of a quasi-ordered crystalline phase which was also observed in another study for the P3HT homopolymer that at high temperature range the π–π stacking interaction between P3HTs is not sufficiently strong enough to maintain a perfect planarity of P3HT chains yet the resulting twisted thiophene units were nonetheless incorporated within the less-ordered quasi-crystalline state.[28] As the temperature further increases to 200 °C, the WAXS patterns show only a weak (100) plane, indicating only a short-range ordering in the P3HT stacking. Therefore, at about 200 °C, the P3HT chains in HTVP20 exhibit a quasi-ordered nematic liquid crystalline structure.[50] Upon further increasing the temperature above 220 °C, the WAXS patterns show no visible diffraction peaks, indicating that the P3HT chains may contain many twisted thienyl units and exhibit a relatively short conjugation length compared with that of the rigid-rod conformation at low temperatures. As a result, the heating process of HTVP20 can be viewed as converting the well-ordered P3HT crystalline phase into the disordered state *via* the quasi-ordered intermediate phase. The temperature at which each phase transition occurs for all P3HT–P2VP block copolymer samples is listed in Table 1 and will be discussed in the following section.

Phase diagram of P3HT–P2VP block copolymers. Based on the combined results of the solid-state UV-VIS, TEM, SAXS and WAXS measurements, a detailed phase diagram of the P3HT–P2VP system in the form of the annealing temperature *versus* its P2VP volume fraction in the strong and weak segregation regimes can now be constructed. As shown in Fig. 9, with a low P2VP fraction of ~0.2, HTVP20 displays a thermodynamically stable nanowire structure with a fully extended rigid rod structure across the width of the nanowires. With increasing temperature, HTVP20 exhibits a smectic-like crystal-to-nematic phase transformation at ~200 °C followed by a nematic-to-isotropic transition at 220 °C, as indicated by the DSC and WAXS measurements. With ϕ = 0.46, HTVP46 exhibits a lamellae structure and its P3HT block exhibits a segmented rod-like structure connected by twisted 3HT units, forming a smectic-like crystal structure within its lamellar domain at low temperature. Upon increasing the annealing temperature, the increased thermal energy allows the more twisting structure between adjacent 3HT units and P3HT adopts a more coil-like structure within their lamellae structure at higher temperature. For all the lamellar structured P3HT–P2VP samples (ϕ = 0.29, 0.46, and 0.57), their P3HT smectic/isotropic transition temperature was found to be lower than their block copolymer order–disorder transition temperature. This result suggests that the P3HT–P2VPs exhibit a smectic-lamellae structure at low temperature, an amorphous-lamellae structure at higher temperature, and a disordered structure above the order–disorder temperature. With an increasing P2VP fraction roughly between ~0.68 and ~0.76, a hexagonal packed cylinder phase (Hex) was observed for the P3HT–P2VP system at low temperatures (<140 °C). Upon heating HTVP68, there is an order–order transformation from a hexagonal cylinder phase to a gyroid phase (G). This gyroid phase appears in only a very narrow range of ϕ ~0.68 since only HTVP68 but not HTVP76 exhibits this transformation. At even higher temperatures, there is an order–disorder transition for both HTVP68 and HTVP76. Finally, HTVP87 exhibits a spherical or disorder micelle phase. A schematic illustration showing how P3HT chains pack within the microphase separated domains is shown in Fig. 10.

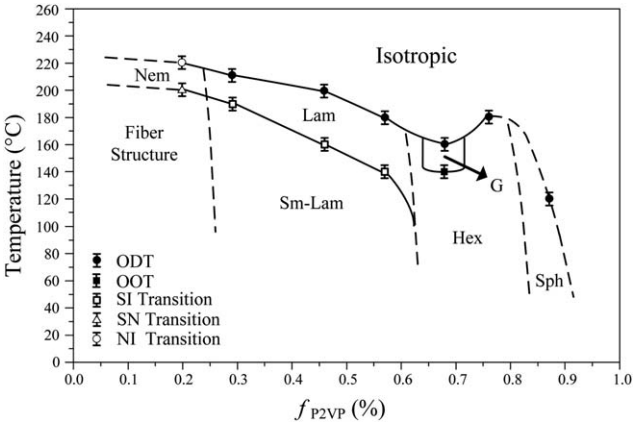

Fig. 9 The phase diagram of the P3HT–P2VP block copolymer system. The notation is explained as follows: (Sph) sphere, (Hex) hexagonal packed cylinders, (G) gyroid phase, (Lam) lamellae, (Sm-Lam) smectic-like lamellae, (Nem) nematic structure, (SI transition) smectic–isotropic transition, (SN transition) smectic–nematic transition, and (NI transition) nematic–isotropic transition.

The self-assembly behavior of P3HT–P2VP block copolymers reveals two important thermodynamic parameters including the

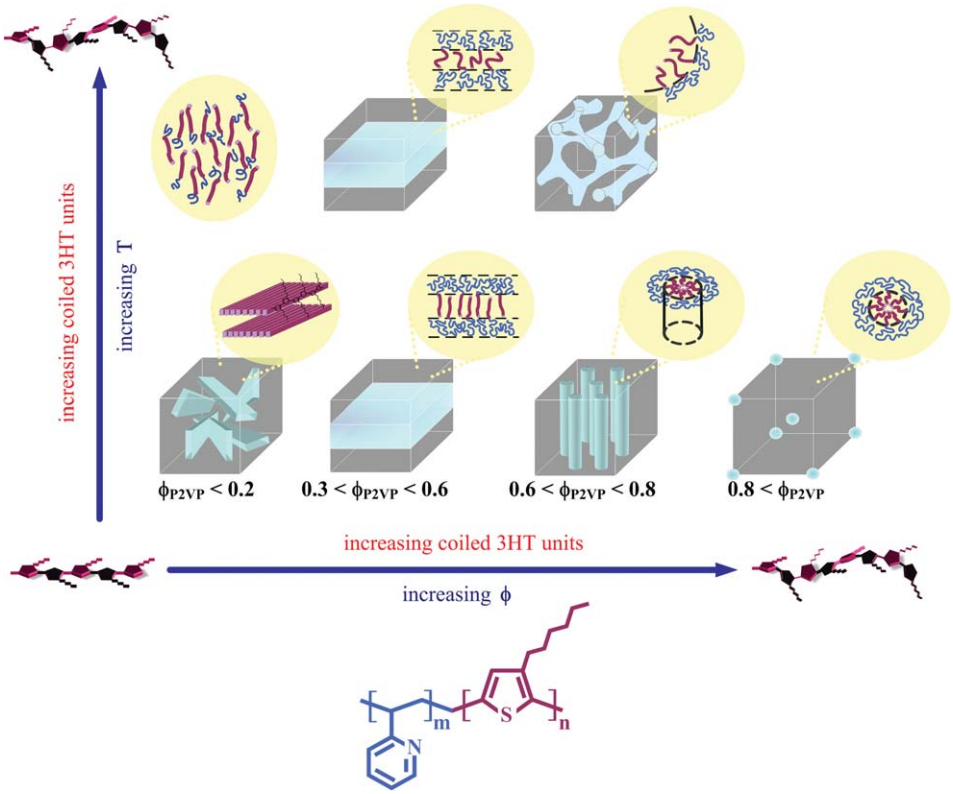

Fig. 10 Schematic representation of the chain conformation of the P3HT–P2VP block copolymers in the microphase separated nanodomains as a function of temperature and composition.

microphase segregation strength and the rod–rod interaction between the conjugated chains that dictate their phase diagram. For P3HT-rich samples, the rod–rod interaction acts as the primary driving force in thermodynamics, and therefore nematic ordering dominates the self-assembly behavior of block copolymers below the isotropic state. Upon further reducing the temperature, the anisotropic ordering induced by the attractive forces between P3HT segments serves to modify the location of chain transition, and subsequently the crystallization effect that favors the formation of parallel oriented bonds leads to a nanowire structure instead of the usual BCC or hexagonal morphologies. With further increasing coil fractions, the presence of microphase separated structures represents the instability of the isotropic–nematic boundary and the self-assembly behavior of the copolymers is mainly driven by the microphase segregation strength. The periodic nanostructures with different compositions reflect the need to minimize the interfacial energy and the amount of stretching that both P2VP as well as the conjugated P3HT chains must sustain in order to fill the space and maintain a uniform segmental density. Within the self-organized nanostructures, the equilibrium molecular packing of P3HT is further moderated by a compromise between the confined environment and the crystallization effect of the semi-rigid chains of P3HT. In the lamellar nanodomains, the increasing rod–rod interaction due to undercooling of the polymers from the amorphous lamellar state improves the anisotropic ordering of P3HT chains, resulting in the P3HT packing along the lamellar structural environment driven by the crystallization process. Therefore, the occurrence of a smectic-like phase, in which P3HT chains are composed of shorter rods connected by twisted 3HT units, can be attributed to the consequence of one dimensional confinement effect on P3HT stacking. However, in the cylindrical and spherical morphologies, parallel packing of P3HT segments without any twisting cannot be achieved due to the high interfacial curvature of the P3HT/P2VP boundary. The chain architecture permits the effect of restricting anisotropic arrangement of P3HT segments prior to crystallization and the two- and three-dimensional nanostructures further inhibit the regular packing of P3HT upon crystallization.

Our experimental results agree qualitatively with the theoretical predictions for rod–coil block copolymer systems. However, significant differences between phase diagrams are found. Theory predicted that the phase diagram for a fully rigid rod–coil block copolymer is highly asymmetrical, with the presence of BCC and hexagonal phases in a rather high coil-rich region.[18] Furthermore, a gyroid phase was not predicted in their phase diagram. In contrast to the thermodynamic behaviors of fully rigid rod–coil block copolymers, the phase diagram of P3HT–P2VP with the P2VP volume fraction above 0.4 bears more resemblance to that of coil–coil block copolymers with conformational asymmetry in which four equilibrium morphologies have been identified: lamellae, bicontinuous gyroid, hexagonally packed cylinders and sphere structures.[51] Considering the semi-rigid nature of P3HT chains, therefore, it is not surprising that the self-assembling behavior of the current block copolymer system containing P3HT exhibits complicated features compared with the previous thermodynamic calculations and simulations, all of which assumed the rod block is a fully rigid rod. Our

experimental results provide new insights into the semirod–coil block copolymer system with adjustable chain stiffness for further future simulation, computation and experiments.

Conclusions

In this study, a series of monodisperse P3HT–P2VP block copolymers was synthesized from P2VP blocks with different molecular weights and a P3HT block with a fixed molecular weight. Therefore, the relative strength of the microphase separation interaction (χN_{total}) to the orientational ordering (μN_{P3HT}) between P3HTs for the self-assembly behavior can be accessed by the change of the molecular weight of the copolymers. Based on the UV and PL measurements, P3HT chains in the solid state undergo a rod-to-coil transition on their main-chain conformation with increasing P2VP molecular weights, indicating that the transition can be facilitated by the rotation of the single carbon–carbon bonds between adjacent 3HT units. Subsequently, TEM, SAXS, WAXS, and DSC were used to explore the detailed phase diagram of the semirod–coil P3HT–P2VP system. These measurements demonstrate that for the strong rod–rod interaction regime ($\mu N_{P3HT} > \chi N_{total}$), the smectic-like nanofibril structure is a thermodynamically stable self-assembled structure for HTVP20 with a low coil fraction. At high temperatures, the smectic-like nanofibers undergo a liquid crystal phase transition to a nematic state followed by the transition to an isotropic phase. The effect of strong orientational ordering between P3HTs can also be seen for the lamellar structured HTVP29 since the block copolymer would exhibit a cylindrical structure if the P3HT chains were to adopt a fully coil-like structure at this volume fraction. With further increasing P2VP molecular weights, the strength of microphase separation interaction prevails over the orientational ordering of P3HTs ($\chi N_{total} > \mu N_{P3HT}$). Therefore P3HT chains adopt a random coil-like structure and the corresponding block copolymers exhibit lamellar, hexagonal, and spherical structures which are typical for coil–coil block copolymer systems. For the lamellae structured P3HT–P2VP, their P3HT blocks undergo a smectic-like to amorphous phase transition below their order–disorder transition temperatures. Additionally, a gyroid phase which is often absent in the rod–coil diblock copolymer system was observed upon heating a HCP structured P3HT–P2VP. The formation of the ordered structures can be attributed to the consequence of energy balance associated with coil stretching, interfacial energy and anisotropic arrangement of P3HT segments. P3HT–P2VPs show overall features in the phase diagram which are both different from those of coil–coil as well as rod–coil block copolymer systems, due to the change in the P3HT chain conformation with composition. As a consequence, the results of this study show promises for practical uses of self-assembling block copolymers containing poly(thiophene) since the resulting phase diagram offers a level of structural control that is important for future applications.

Acknowledgements

The financial support from the National Science Council of Taiwan is greatly appreciated. The X-ray measurements were conducted in Taiwan at the National Synchrotron Radiation Research Center (NSRRC). The authors would also like to thank Dr U-Ser Jeng and Dr Ming-Tao Lee for their help during the X-ray experiments at NSRRC.

Notes and references

1 A. Kraft, A. C. Grimsdale and A. B. Holmes, *Angew. Chem., Int. Ed.*, 1998, **37**, 402–428.
2 M. T. Bernius, M. Inbasekaran, J. O'Brien and W. S. Wu, *Adv. Mater.*, 2000, **12**, 1737–1750.
3 F. J. M. Hoeben, P. Jonkheijm, E. W. Meijer and A. P. H. J. Schenning, *Chem. Rev.*, 2005, **105**, 1491–1546.
4 J. S. Liu, T. Tanaka, K. Sivula, A. P. Alivisatos and J. M. J. Frechet, *J. Am. Chem. Soc.*, 2004, **126**, 6550–6551.
5 G. Li, V. Shrotriya, J. S. Huang, Y. Yao, T. Moriarty, K. Emery and Y. Yang, *Nat. Mater.*, 2005, **4**, 864–868.
6 H. Sirringhaus, *Adv. Mater.*, 2005, **17**, 2411–2425.
7 P. Leclere, V. Parente, J. L. Bredas, B. Francois and R. Lazzaroni, *Chem. Mater.*, 1998, **10**, 4010–4014.
8 X. L. Chen and S. A. Jenekhe, *Macromolecules*, 2000, **33**, 4610–4612.
9 H. B. Wang, H. H. Wang, V. S. Urban, K. C. Littrell, P. Thiyagarajan and L. P. Yu, *J. Am. Chem. Soc.*, 2000, **122**, 6855–6861.
10 G. Cho, M. Jung, H. Yang, J. H. Song and M. M. Sung, *Langmuir*, 2006, **22**, 4896–4898.
11 C. Muller, S. Goffri, D. W. Breiby, J. W. Andreasen, H. D. Chanzy, R. A. J. Janssen, M. M. Nielsen, C. P. Radano, H. Sirringhaus, P. Smith and N. Stingelin-Stutzmann, *Adv. Funct. Mater.*, 2007, **17**, 2674–2679.
12 B. W. Boudouris, C. D. Frisbie and M. A. Hillmyer, *Macromolecules*, 2008, **41**, 67–75.
13 Y.-H. Lee, C.-J. Chang, C.-J. Kao and C.-A. Dai, *Langmuir*, 2010, **26**, 4196–4206.
14 K. Sivula, Z. T. Ball, N. Watanabe and J. M. J. Frechet, *Adv. Mater.*, 2006, **18**, 206–210.
15 I. Botiz and S. B. Darling, *Macromolecules*, 2009, **42**, 8211–8217.
16 R. Holyst and M. Schick, *J. Chem. Phys.*, 1992, **96**, 730–740.
17 C. Singh, M. Goulian, A. J. Liu and G. H. Fredrickson, *Macromolecules*, 1994, **27**, 2974–2986.
18 M. Reenders and G. ten Brinke, *Macromolecules*, 2002, **35**, 3266–3280.
19 M. Muller and M. Schick, *Macromolecules*, 1996, **29**, 8900–8903.
20 M. W. Matsen and C. Barrett, *J. Chem. Phys.*, 1998, **109**, 4108–4118.
21 V. Pryamitsyn and V. Ganesan, *J. Chem. Phys.*, 2004, **120**, 5824–5838.
22 B. D. Olsen and R. A. Segalman, *Macromolecules*, 2005, **38**, 10127–10137.
23 B. D. Olsen and R. A. Segalman, *Macromolecules*, 2007, **40**, 6922–6929.
24 N. Sary, L. Rubatat, C. Brochon, G. Hadziioannou, J. Ruokolainen and R. Mezzenga, *Macromolecules*, 2007, **40**, 6990–6997.
25 C.-C. Ho, Y.-H. Lee, C.-A. Dai, R. A. Segalman and W.-F. Su, *Macromolecules*, 2009, **42**, 4208–4219.
26 Y. Huang, H. Cheng and C. C. Han, *Macromolecules*, 2010, **43**, 10031–10037.
27 K. Faid, M. Frechette, M. Ranger, L. Mazerolle, I. Levesque, M. Leclerc, T. A. Chen and R. D. Rieke, *Chem. Mater.*, 1995, **7**, 1390–1396.
28 C. Yang, F. P. Orfino and S. Holdcroft, *Macromolecules*, 1996, **29**, 6510–6517.
29 J. S. Liu, E. Sheina, T. Kowalewski and R. D. McCullough, *Angew. Chem., Int. Ed.*, 2002, **41**, 329–332.
30 M. C. Iovu, C. R. Craley, M. Jeffries-El, A. B. Krankowski, R. Zhang, T. Kowalewski and R. D. McCullough, *Macromolecules*, 2007, **40**, 4733–4735.
31 M. C. Iovu, M. Jeffries-El, R. Zhang, T. Kowalewski and R. D. Mccullough, *J. Macromol. Sci., Part A: Pure Appl. Chem.*, 2006, **43**, 1991–2000.
32 Y. K. Fang, C. L. Liu, C. X. Li, C. J. Lin, R. Mezzenga and W. C. Chen, *Adv. Funct. Mater.*, 2010, **20**, 3012–3024.
33 A. Takahashi, Y. Rho, T. Higashihara, B. Ahn, M. Ree and M. Ueda, *Macromolecules*, 2010, **43**, 4843–4852.
34 T. Higashihara and M. Ueda, *Macromolecules*, 2009, **42**, 8794–8800.
35 M. Sommer, A. S. Lang and M. Thelakkat, *Angew. Chem., Int. Ed.*, 2008, **47**, 7901–7904.

36 T. Higashihara, K. Ohshimizu, A. Hirao and M. Ueda, *Macromolecules*, 2008, **41**, 9505–9507.
37 Z. Q. Wu, R. J. Ono, Z. Chen and C. W. Bielawski, *J. Am. Chem. Soc.*, 2010, **132**, 14000–14001.
38 G. Sauve and R. D. McCullough, *Adv. Mater.*, 2007, **19**, 1822–1825.
39 C.-A. Dai, W.-C. Yen, Y.-H. Lee, C.-C. Ho and W.-F. Su, *J. Am. Chem. Soc.*, 2007, **129**, 11036–11038.
40 R. Zhang, B. Li, M. C. Iovu, M. Jeffries-El, G. Sauve, J. Cooper, S. J. Jia, S. Tristram-Nagle, D. M. Smilgies, D. N. Lambeth, R. D. McCullough and T. Kowalewski, *J. Am. Chem. Soc.*, 2006, **128**, 3480–3481.
41 R. Borsali, S. Lecommandoux, R. Pecora and H. Benoit, *Macromolecules*, 2001, **34**, 4229–4234.
42 D. A. Hajduk, P. E. Harper, S. M. Gruner, C. C. Honeker, G. Kim, E. L. Thomas and L. J. Fetters, *Macromolecules*, 1994, **27**, 4063–4075.
43 E. W. Cochran, C. J. Garcia-Cervera and G. H. Fredrickson, *Macromolecules*, 2006, **39**, 2449–2451.
44 S. Forster, A. K. Khandpur, J. Zhao, F. S. Bates, I. W. Hamley, A. J. Ryan and W. Bras, *Macromolecules*, 1994, **27**, 6922–6935.
45 M. Sundberg, O. Inganas, S. Stafstrom, G. Gustafsson and B. Sjogren, *Solid State Commun.*, 1989, **71**, 435–439.
46 T. J. Prosa, M. J. Winokur, J. Moulton, P. Smith and A. J. Heeger, *Macromolecules*, 1992, **25**, 4364–4372.
47 A. Zen, M. Saphiannikova, D. Neher, J. Grenzer, S. Grigorian, U. Pietsch, U. Asawapirom, S. Janietz, U. Scherf, I. Lieberwirth and G. Wegner, *Macromolecules*, 2006, **39**, 2162–2171.
48 G. W. Heffner and D. S. Pearson, *Macromolecules*, 1991, **24**, 6295–6299.
49 V. Causin, C. Marega, A. Marigo, L. Valentini and J. M. Kenny, *Macromolecules*, 2005, **38**, 409–415.
50 K. Yazawa, Y. Inoue, T. Yamamoto and N. Asakawa, *Phys. Rev. B: Condens. Matter Mater. Phys.*, 2006, **74**, 094204.
51 M. W. Matsen and M. Schick, *Macromolecules*, 1994, **27**, 4014–4015.

